Front. Mech. Eng. 2017, 12(1): 132–142
DOI 10.1007/s11465-017-0436-z

RESEARCH ARTICLE

Ming FENG, Yongbo WU, Julong YUAN, Zhao PING

Processing of high-precision ceramic balls with a spiral V-groove plate

Abstract As the demand for high-performance bearings gradually increases, ceramic balls with excellent properties, such as high accuracy, high reliability, and high chemical durability used, are extensively used for high-performance bearings. In this study, a spiral V-groove plate method is employed in processing high-precision ceramic balls. After the kinematic analysis of the ball-spin angle and enveloped lapping trajectories, an experimental rig is constructed and experiments are conducted to confirm the feasibility of this method. Kinematic analysis results indicate that the method not only allows for the control of the ball-spin angle but also uniformly distributes the enveloped lapping trajectories over the entire ball surface. Experimental results demonstrate that the novel spiral V-groove plate method performs better than the conventional concentric V-groove plate method in terms of roundness, surface roughness, diameter difference, and diameter decrease rate. Ceramic balls with a G3-level accuracy are achieved, and their typical roundness, minimum surface roughness, and diameter difference are 0.05, 0.0045, and 0.105 μm, respectively. These findings confirm that the proposed method can be applied to high-accuracy and high-consistency ceramic ball processing.

Keywords bearing, ceramic ball, spiral V-groove, kinematic analysis, trajectory

1 Introduction

The demand for high-accuracy, high-efficiency, and high-automation machinery is increasing concomitant with the rapid development of the industrial technology. As indispensable components of machinery, bearings determine the accuracy, performance, life span, and reliability of the host machine; therefore, the development of the bearing industry is necessary [1–3]. However, traditional metal bearings can hardly meet the requirements when the working conditions demand high precision and high stability as well as involve high overload, high temperature, and acidic environment. Under these conditions, wherein defects in rolling bodies and raceway are likely to occur, metal bearings are recommended to be replaced by ceramic ones, whose excellent properties include low density, high hardness, high wear resistance, and high corrosion resistance [4–6]. In recent years, ceramic bearings have been extensively applied in aerospace, precision machinery, petrochemical industry, national defense, and other fields. Consequently, the demand for high-precision ceramic balls increases along with the extensive application of ceramic bearings. Ceramic balls are widely used as the rolling bodies for bearings; thus, their precision must reach at least the G5 level. The details of the precision ball grades are listed in Table 1. Furthermore, as an important factor in bearing performance, high-precision ceramic balls present high commercial profit because their commercial demand increases by 15% each year [6]. However, ensuring the quality of high-precision ceramic balls is challenging due to the different precision levels of semi-finished products and the difficulty of manufacturing ceramic balls. This issue provides a significant opportunity to conduct research on the processing of high-precision ceramic balls.

In general, the following two key points must be satisfied in high-precision ceramic ball processing: 1) The different points on the ball surface must have the same probability of being processed; 2) the processing of balls that are of relatively large in size should be given priority. Generally, different processing methods vary in their capability to satisfy these two points: The stronger the capability of the method is, the higher the ball quality

Received September 5, 2016; accepted January 6, 2017

Ming FENG (✉), Yongbo WU
Department of Machine Intelligence & Systems Engineering, Akita Prefectural University, Akita 015-0055, Japan
E-mail: fengming995@163.com

Julong YUAN, Zhao PING
Ultra-Precision Machining Center, Zhejiang University of Technology, Hangzhou 310014, China

Table 1 Precision ball standards

Level	Deviation from spherical form: Roundness/μm	Surface roughness/μm	Lot variation diameter/μm
G3	0.08	0.012	0.13
G5	0.13	0.020	0.25
G10	0.25	0.025	0.50

becomes. In other words, the processing method significantly influences the ball quality. Currently, the traditional metal ball processing methods are mainly utilized to produce high-accuracy ceramic balls, including concentric/eccentric V-groove plate method, controllable ball-spin angle method, and magnetic abrasive slurry processing method. In the controllable ball-spin angle method, the V-grooves are separate, and the sole concentric V-groove is formed by the inner and outer plates. The ball-spin angle is used to describe the self-motion behavior of the ball, and a dynamic ball-spin angle can result in an enveloped lapping trajectories over the ball surface [7,8].

In the concentric V-groove plate method [9,10], the ball-spin angle is kept constant during processing, and a stirring device is utilized to realize a randomly changeable ball-spin angle. The eccentric V-groove method achieves a dynamic ball-spin angle by setting an eccentric distance between the upper and lower plates [11]. Although this technique improves ball roundness, it increases the diameter deviation and requires high installation precision of the employed machine. Controllable ball-spin angle by the separated V-groove method was proposed to control the ball-spin angle accurately. In this method, the velocity difference between the inner and outer plates are generated; however, the quantity of balls that can be simultaneously machined in a batch is limited by having only one V-groove [12]. In the magnetic abrasive slurry processing method, a slurry produced by blending abrasives into a magnetic fluid is used to process the balls. This method considerably improves the material removal rate during processing in the given magnetic field [13,14].

The processing of high-precision ceramic balls should simultaneously meet the following requirements: Large-scale processing and high accuracy. In terms of processing cost, the concentric V-groove plate method is the best method. Aside from low processing cost, it is also widely adopted because of it presents a simple mechanical structure, accommodates large-scale processing. However, its drawback is its requirement for a stirring device to change the ball-spin angle randomly for the achievement of an enveloped lapping trajectory [15]. Zhao et al. [16] proposed a new method that can achieve high accuracy, high consistency, circular processing, and variable ball-spin angle in one cycle by substituting the concentric V-groove plate with variable-radius V-groove plate and using a recycler for balls. This technique has been successfully applied in steel ball processing. However, only few studies on ceramic ball processing have been conducted using this new method. In this study, we draw on the method of Zhao et al. [16] to develop a novel precision processing technique for ceramic balls. In our proposed method, a spiral V-groove plate is used to replace the concentric V-groove plate. We conduct a kinematic analysis of the ball-spin angles in two directions as well as ceramic ball processing experiments to confirm the validity of the proposed processing technique.

2 Ball processing with a spiral V-groove plate

Figure 1 shows the schematic diagram of the system for the proposed ball processing technique. As shown, an Archimedes spiral V-groove plate is used. The upper plate with a spiral V-groove is placed on top of the flat lower plate. In addition, a loading mechanism and a recycler are attached to the upper plate. At a certain distance to the center of the upper plate, an inclined through-hole is machined in the upper plate and used as the

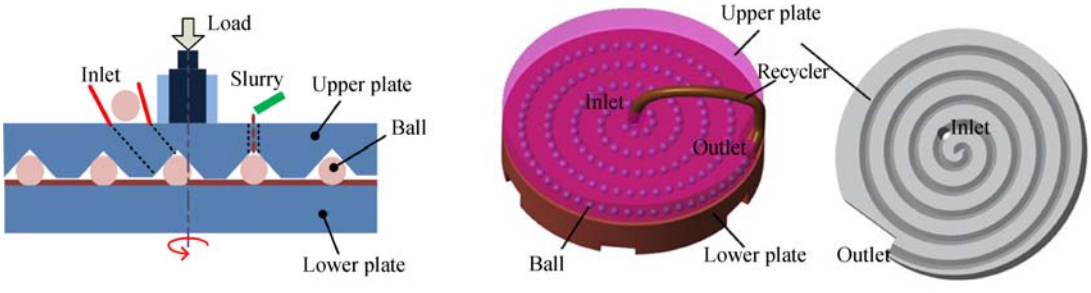

Fig. 1 Ball processing with a spiral V-groove plate

inlet for the balls. The outlet is located at the edge of the lower plate. A recycler, which links the inlet to the outlet, supplies the balls to be processed through the inlet and collects the balls processed from the outlet. If necessary, the recycler is used to supply and collect the balls in the next cycle of processing. A cycle is completed when a ceramic ball passes through the inlet to the processing zone and exits the outlet. A motor supplies the power that drives the lower plate to rotate. During processing, the materials of the workpieces are removed to improve the ball roundness and surface roughness by the combined effects of loading, rotation, and slurry.

2.1 Ball-spin angles

Figures 2(a)–2(d) show the schematics of the instantaneous geometric relationship between the ball and the plates at an arbitrary moment during processing and the kinematic analysis. On the assumption that a polar coordinate system $RO_0\varphi$ is fixed on the upper plate and the origin of which is at the center O_0 of the working surface of the upper plate, the equation for the spiral that describes the motion track of the balls and the track of the V-groove simultaneously is given by $R = a\varphi$ ($\varphi_0 < \varphi < \varphi_e$). In this equation, a is a constant, and φ_0 and φ_e represent the polar angles determining the initial and end points of the spiral, respectively (Fig. 2(a)). When φ is equal to 0, the ball enters the processing zone from the center of the upper plate. As φ increases, the ball moves forward along the spiral. As shown in Figs. 2(a) and 2(b), the upper and lower plates are installed concentrically, that is, Point O_0 and the center Point O of the working surface of the lower plate are on the same vertical line. A is the contact point of the ball with the lower plate, whereas B and C are contact points of the ball both sides of the V-groove with the angles of α and β on the upper plate. In Fig. 2(a), ρ_A, ρ_B, and ρ_C are the curve radii of the spiral tracks at contact Points A, B, and C, respectively; P_A, P_B, and P_C are the centers of the curve radii ρ_A, ρ_B, and ρ_C, respectively.

A rectangular coordinate system XYZ is fixed on the ball with a radius of r_b, and the origin of this coordinate system is located at the geometric center O_b of the ball, as shown in Fig. 2(c). In the same figure, $\boldsymbol{\Omega}_s$ denotes the ball-spin angular speed vector, which is divided into two vectors, namely, $\boldsymbol{\Omega}_b$ and $\boldsymbol{\Omega}_g$ in XY-plane and Z-axis, respectively. The angles between $\boldsymbol{\Omega}_b$ and the X-axis and between $\boldsymbol{\Omega}_g$ and

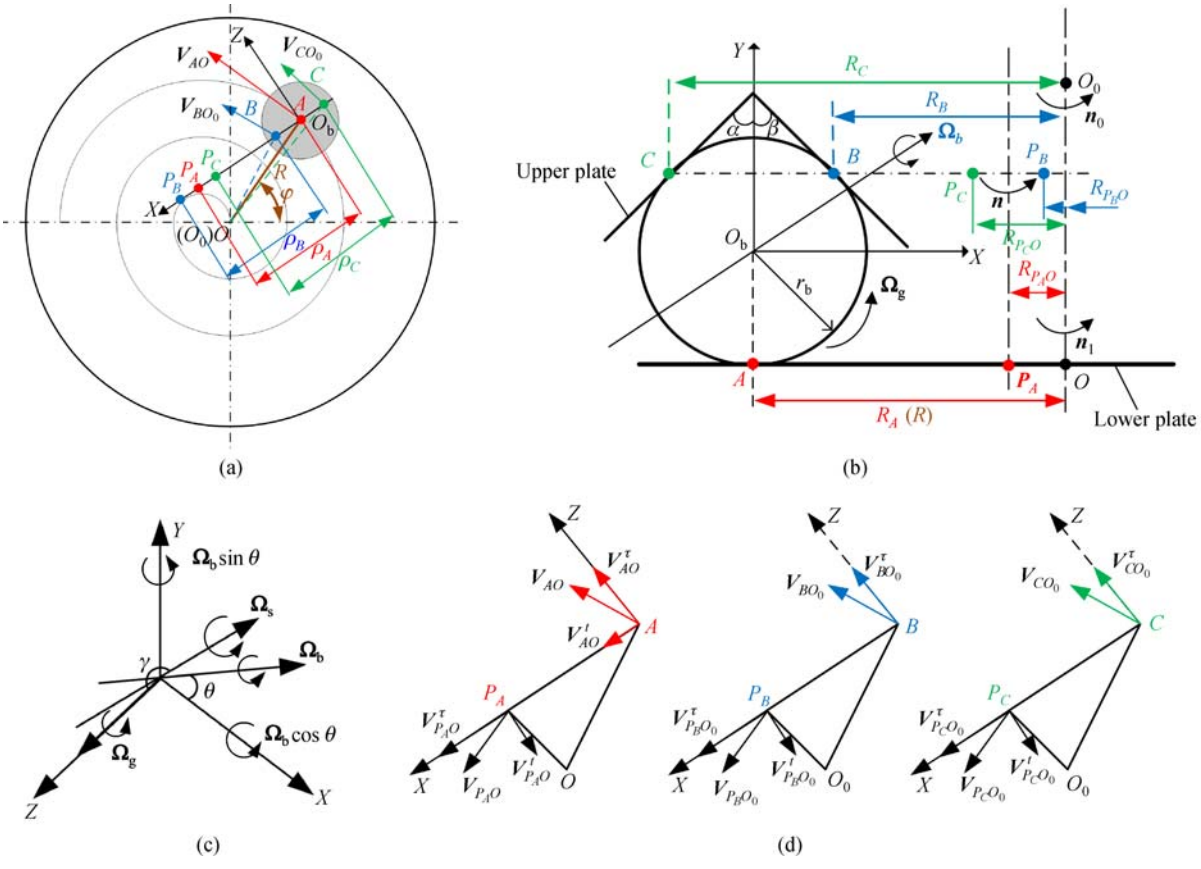

Fig. 2 Schematics of the geometric relationship between the ball and plates and the kinematic analysis. (a) The major view of geometric relationship between the ball and plates; (b) the side view of geometric relationship between the ball and plates; (c) the coordinate for defining ball-spin angular speed vectors; (d) velocity analysis of different points

$\boldsymbol{\Omega}_s$ are denoted by θ and γ, which are regarded as the ball-spin angles. Moreover, the angular rotation speeds of the ball around X-, Y-, and Z-axes are given by $\boldsymbol{\Omega}_b\cos\theta$, $\boldsymbol{\Omega}_b\sin\theta$, and $\boldsymbol{\Omega}_g$, respectively. The angular rotation speeds of the upper and lower plates are denoted by n_0 and n_1, respectively. The angular rotation speed of the geometric center of the ball around the axis that is vertical to the lower plate and intersects the lower plate at Point P_A is denoted by n. The distance between Points A and O is R_A, and the distances of Points B and C to Point O_0 are R_B and R_C, respectively. The velocities of Points A, B, and C and those of P_A, P_B, and P_C can be divided into two components in the X- and Z-axes, respectively, as shown in Fig. 2(d). The following assumptions of pure rolling motion are considered in the analysis:

1) The pushing and impact forces between balls are ignored;

2) The slide motions between the balls and plates are disregarded;

3) All the components are regarded as rigid bodies.

Subsequently, the velocity balance equations are obtained as follows:

$$\begin{cases} \overline{\boldsymbol{V}^{\tau}_{AP_A}} = \overline{\boldsymbol{V}^{\tau}_{AO_b}} + \overline{\boldsymbol{V}^{\tau}_{O_bO}} - \overline{\boldsymbol{V}^{\tau}_{P_AO}} \\ \overline{\boldsymbol{V}^{\tau}_{BP_B}} = \overline{\boldsymbol{V}^{\tau}_{BO_b}} + \overline{\boldsymbol{V}^{\tau}_{O_bO}} - \overline{\boldsymbol{V}^{\tau}_{P_BO}} \\ \overline{\boldsymbol{V}^{\tau}_{CP_C}} = \overline{\boldsymbol{V}^{\tau}_{CO_b}} + \overline{\boldsymbol{V}^{\tau}_{O_bO}} - \overline{\boldsymbol{V}^{\tau}_{P_CO}} \\ \overline{\boldsymbol{V}^{t}_{AP_A}} = \overline{\boldsymbol{V}^{t}_{AO_b}} + \overline{\boldsymbol{V}^{t}_{O_bO}} - \overline{\boldsymbol{V}^{t}_{P_AO}} \end{cases}.$$

The absolute velocity of the ball center point O_b can be expressed by $\boldsymbol{V}_{O_bO} = R_A\boldsymbol{n}_1$; thus, the projection velocities along the X- and Z-axes are $\boldsymbol{V}^{t}_{O_bO} = R_A\boldsymbol{n}_1\sin(\angle P_AAO)$ and $\boldsymbol{V}^{\tau}_{O_bO} = R_A\boldsymbol{n}_1\cos(\angle P_AAO)$, respectively. The absolute velocity expression of Point P_A is $\boldsymbol{V}_{P_AO} = R_{P_A}\boldsymbol{n}_1$; thus, its projection velocities along the X- and Z-axes are $\boldsymbol{V}^{t}_{P_AO} = R_{P_A}\boldsymbol{n}_1\sin(\angle AP_AO)$ and $\boldsymbol{V}^{\tau}_{P_AO} = R_{P_A}\boldsymbol{n}_1\cos(\angle AP_AO)$, respectively. $\boldsymbol{\Omega}_b$ induced relative velocity of Points A to O_b is $\overline{\boldsymbol{V}^{\tau}_{AO_b}}$, and the relative velocity caused by $\boldsymbol{\Omega}_g$ is $\overline{\boldsymbol{V}^{t}_{AO_b}}$; $\boldsymbol{V}^{\tau}_{AP_A} = \rho_A\boldsymbol{n}$, and $\boldsymbol{V}^{t}_{AP_A} = 0$. By the way, $\boldsymbol{n}_0$, $\boldsymbol{n}_1$ represent the angular speed of upper and lower plate and $\boldsymbol{n}$ is the revolution speed of the ball. Subsequently, the same definitions are applied to the rest of the contact points. Finally, the equations are deduced on the basis of the velocity balance equations and given by

$$\begin{cases} \rho_A\boldsymbol{n} = r_b\boldsymbol{\Omega}_b\cos\theta + R_A\boldsymbol{n}_1\cos(\angle P_AAO) \\ \qquad +R_{P_AO}\boldsymbol{n}_1\cos(\angle AP_AO) \\ \rho_B\boldsymbol{n} = -r_b\boldsymbol{\Omega}_b\sin(\beta-\theta) + R_B\boldsymbol{n}_0\cos(\angle P_BBO) \\ \qquad +R_{P_BO}\boldsymbol{n}_0\cos(\angle BP_BO) \\ \rho_C\boldsymbol{n} = -r_b\boldsymbol{\Omega}_b\sin(\alpha+\theta) + R_C\boldsymbol{n}_0\cos(\angle P_CCO) \\ \qquad +R_{P_CO}\boldsymbol{n}_0\cos(\angle CP_CO) \\ 0 = r_b\boldsymbol{\Omega}_g + R_A\boldsymbol{n}_1\sin(\angle P_AAO) - R_{P_AO}\boldsymbol{n}_1\sin(\angle AP_AO) \end{cases}. \tag{1}$$

During this process, the upper plate is fixed; thus, $\boldsymbol{n}_0 = 0$, and α is equal to β. The relationships between the parameters in Eq. (1) are defined by the following equations:

1) Curve radius

$$\rho_C = r_b\cos\alpha + \rho_A, \tag{2}$$

$$\rho_B = \rho_A - r_b\cos\beta. \tag{3}$$

2) Angles

$$\cos(\angle P_AAO) = \frac{\rho_A^2 + R_A^2 - P_AO^2}{2\rho_AR_A}, \tag{4}$$

$$\cos(\angle AP_AO) = \frac{\rho_A^2 - R_A^2 + P_AO^2}{2\rho_AR_{P_AO}}. \tag{5}$$

Substituting Eqs. (2)–(5) into Eq. (1) yields the following kinematic equations:

$$\begin{cases} \theta = \arctan\dfrac{r_b\sin\alpha}{\rho_A} \\ \boldsymbol{\Omega}_b = -\dfrac{R_A\boldsymbol{n}_1\cos(\angle O_AAO) + R_{P_AO}\boldsymbol{n}_1\cos(\angle AO_AO)}{r_b\cos\theta(\sin\alpha+1)} \\ \boldsymbol{n} = \dfrac{(R_A\boldsymbol{n}_1\cos(\angle O_AAO) + R_{P_AO}\boldsymbol{n}_1\cos(\angle AO_AO))\sin\alpha}{\rho_A(\sin\alpha+1)} \\ \boldsymbol{\Omega}_g = \dfrac{-R_A\boldsymbol{n}_1\sin(\angle O_AAO) + R_{P_AO}\boldsymbol{n}_1\sin(\angle AO_AO)}{r_b} \end{cases}. \tag{6}$$

Subsequently, the angle γ is obtained and represented by

$$\gamma = \arctan\frac{\boldsymbol{\Omega}_b}{\boldsymbol{\Omega}_g} = \arctan\frac{R_A\cos(\angle O_AAO) + R_{P_AO}\cos(\angle AO_AO)}{(-R_A\sin(\angle O_AAO) + R_{P_AO}\sin(\angle AO_AO))\cos\theta(\sin\alpha+1)}. \tag{7}$$

According to Eq. (6) the curve radius ρ_A and the distance of P_A to O are required to obtain the ball-spin angles. Both of these parameters can be obtained by the following equations [17]:

$$\rho_A = \frac{(1+\varphi^2)^{3/2}}{2+\varphi^2}, \tag{8}$$

$$R_{P_AO} = \left\| \frac{Re^{i\varphi} + e^{-i\varphi}R^2(a-R)}{R^2 + 2a^2} \right\|. \quad (9)$$

Finally, the numerical solution of the spin angles can be performed using the given values of some parameters. The simulation results are presented and discussed in Section 2.3.

2.2 Enveloped lapping trajectories

The ball-spin angles have been obtained in the previous section. In this section, the method by which to calculate the trajectories of contact Points A, B, and C during processing is explained. The initial coordinates of Points A, B, and C are $(0, -r_b, 0)$, $(r_b\cos\alpha, r_b\sin\alpha, 0)$, and $(-r_b\cos\beta, r_b\sin\beta, 0)$, in the rectangular coordinate system XYZ, respectively. They are transformed into the new coordinates N_A, N_B, and N_C, which are expressed as follows:

$$\begin{cases} N_A = [0, -r_b, 0]^T \\ N_B = [r_b\cos\alpha, r_b\sin\alpha, 0]^T \\ N_C = [-r_b\cos\beta, r_b\sin\beta, 0]^T \end{cases}. \quad (10)$$

In addition, the rotation angle expressions are as follows:

$$\begin{cases} \overline{\zeta}_x(i+1) = \zeta_x(i) + \overline{\zeta}_x(i) \\ \overline{\zeta}_y(i+1) = \zeta_y(i) + \overline{\zeta}_y(i) \\ \overline{\zeta}_z(i+1) = \zeta_z(i) + \overline{\zeta}_z(i) \end{cases}, \quad (11)$$

where i is the serial number of sampling time, $\overline{\zeta}_x(i+1)$ is the next value of the rotation angle $\overline{\zeta}_x(i)$, and $\zeta_x(i)$ is the increment of the rotation angle at the current moment. The same explanation applies to the rest. The value of the increment is obtained as follows:

$$\begin{cases} \zeta_x(i) = |\boldsymbol{\Omega}_b\cos\theta(i)|\Delta t \\ \zeta_y(i) = |\boldsymbol{\Omega}_b\sin\theta(i)|\Delta t \\ \zeta_z(i) = |\boldsymbol{\Omega}_g|\Delta t \end{cases}, \quad (12)$$

where Δt is the step interval calculated by

$$\Delta t = \frac{\varphi(i+1) - \varphi(i)}{n(i)}. \quad (13)$$

The rotational coordinate transformation matrix around each axis is expressed as

$$\begin{cases} X_{rot} = \begin{bmatrix} 1 & 0 & 0 \\ 0 & \cos\overline{\zeta}_x(i+1) & -\sin\overline{\zeta}_x(i+1) \\ 0 & -\sin\overline{\zeta}_x(i+1) & \cos\overline{\zeta}_x(i+1) \end{bmatrix} \\ Y_{rot} = \begin{bmatrix} \cos\overline{\zeta}_y(i+1) & 0 & \sin\overline{\zeta}_y(i+1) \\ 0 & 1 & 0 \\ -\sin\overline{\zeta}_y(i+1) & 0 & -\cos\overline{\zeta}_y(i+1) \end{bmatrix} \\ Z_{rot} = \begin{bmatrix} \cos\overline{\zeta}_z(i+1) & -\sin\overline{\zeta}_z(i+1) & 0 \\ \sin\overline{\zeta}_z(i+1) & \cos\overline{\zeta}_z(i+1) & 0 \\ 0 & 0 & 1 \end{bmatrix} \end{cases}. \quad (14)$$

Finally, the coordinates of the contact points at each step interval can be calculated by

$$\begin{cases} N_A(i+1) = Y_{rot}X_{rot}Z_{rot}N_A(i) \\ N_B(i+1) = Y_{rot}X_{rot}Z_{rot}N_B(i) \\ N_C(i+1) = Y_{rot}X_{rot}Z_{rot}N_C(i) \end{cases}. \quad (15)$$

The coordinates of the contact points are obtained and transformed from rectangular coordinates to spherical coordinates by using the above calculation. The trajectories of the contact points are subsequently deduced.

2.3 Analysis results and discussion

In practice, r_b and α are constant; thus, the θ value based on the θ expression in Eq. (6) only varies with the curve radius ρ_A, whose values differ across different positions along the track of the spiral V-groove. In other words, θ can be controlled by the curve radius. By contrast, γ (Eq. (7)) depends on several variable parameters, and its control is relatively complex compared with θ.

The ball-spin angles θ and γ and the enveloped lapping trajectories are obtained using Eqs. (10)–(15) and the processing parameters listed in Table 2. For comparison, the ball-spin angle and enveloped lapping trajectories in the conventional concentric V-groove method are also obtained using Eq. (16) [18] and Eqs. (10)–(15), respectively. The stop conditions applied to end the simulation for the concentric V-groove plate and the spiral V-groove plate are $\varphi = 2\pi$ (one revolution) and $\varphi = 18\pi$

Table 2 Processing parameters for kinematic analysis

Plate	Track of V-groove	Ball diameter/mm	$\alpha = \beta$/rad	Rotation speed/(r·min^{-1})	Stop condition
Concentric V-groove plate	$R = 100$ $(0 < \varphi < 2\pi)$	5	$\pi/4$	$n_0 = 0$, $n_1 = 45$	$\varphi = 2\pi$
Spiral V-groove plate	$R = 1.82\varphi$ $(0 < \varphi < 18\pi)$	5	$\pi/4$	$n_0 = 0$, $n_1 = 45$	$\varphi = 18\pi$

(ball exits from the outlet), respectively.

$$\theta = \arctan\left(\frac{r_b}{R_A}\sin\alpha\right), \tag{16}$$

where the R_A is the radius of a circle along the tip of the concentric V-groove.

Figures 3(a) and 3(b) show that the obtained ball-spin angle and enveloped lapping trajectories in the conventional concentric V-groove plate method, respectively. In Fig. 3(b), the enveloped lapping trajectories of contact Points A, B, C are color coded in red, green, and blue, respectively. The ball-spin angle remains the same during processing because the V-groove radius is constant at R_A (Eq. (16)) and the trajectory of each contact point is round. These results demonstrate that the ball-spin angle behaves invariably at 2.4°, and the enveloped lapping trajectories are only three circles over the ball surface, confirming that a stirring device is essential for ball processing in the conventional concentric V-groove plate method for the uniform distribution of the enveloped lapping trajectories over the entire ball surface.

Figures 4(a) and 4(b) show the theoretically obtained two ball-spin angles and enveloped lapping trajectories in the spiral V-groove plate method, respectively. As shown in Fig. 4(a), θ initially rapidly decreases from 90° to 10° within a short processing time and subsequently slightly changes. The ball-spin angle γ varies between $-90°$ and 90° at the beginning and then almost remained constant at around 82°. For the enveloped lapping trajectories of contact Points A, B, and C, Fig. 4(b) shows that the lapping trajectories can uniformly envelope the entire ball surface in only one cycle. Thus, this new method generally has the capacity to control the ball-spin angle and uniformly envelope the entire ball surface with the lapping trajectories in only one cycle.

3 Experiments

3.1 Experimental rig, conditions, and procedure

An experimental rig was constructed by replacing the concentric V-groove plate with a spiral V-groove plate and attaching a cycler onto the existing concentric V-groove plate-type ball-processing machine, as shown in Fig. 5(a). This experimental rig is used to confirm the kinematic analysis in the previous section and validate the performance of the new method in the precision processing of ceramic balls. In this study, two rounds of experiments were designed and conducted on the constructed rig. The first test was conducted to validate the new method, in which the spiral V-groove with the following track expression was used:

$$R = 1.82\varphi \ (7\pi<\varphi<14\pi). \tag{17}$$

Figure 5(b) presents a picture of the spiral V-groove plate, which was made from cast iron. It was 300 mm in diameter and 30 mm in thickness. The V-groove had an 8 mm width, 8 mm depth, and 45° α and β angles. For comparison, experiments were also performed using a concentric V-groove plate (Fig. 5(c)) with V-grooves that are same in structure and dimensions as those on the spiral V-groove plate. However, unlike in the spiral V-groove plate method, in which the V-groove plate was used as the upper plate, the V-groove plate was used as the lower plate, and a hole was created in the upper plate for the artificial stirring of the ball-spin angle in the concentric V-groove plate method.

The second round of experiments were conducted to elucidate the potential of the new method for the high-accuracy processing of ceramic balls. In this round, the spiral V-groove with the following track equation was utilized:

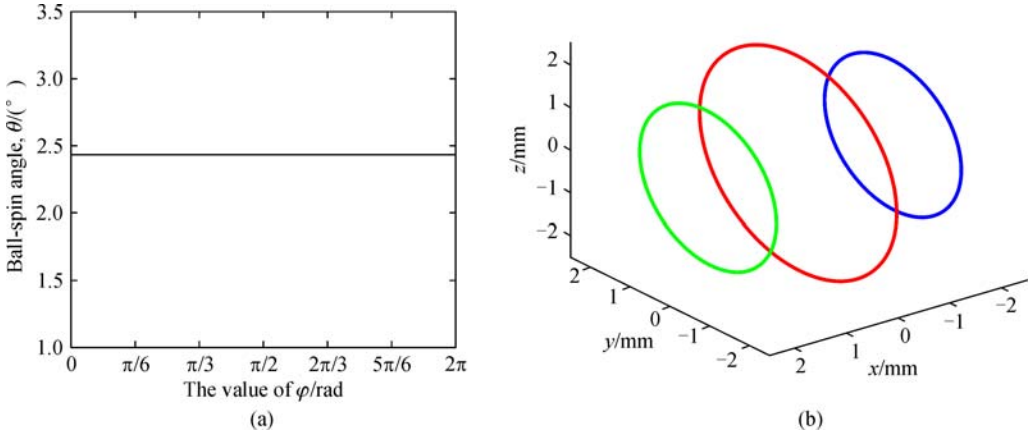

Fig. 3 Ball-spin angle and enveloped lapping trajectories in the conventional concentric V-groove plate method. (a) Ball-spin angle; (b) enveloped lapping trajectories (the enveloped lapping trajectories of contact Points A, B, and C are color coded in red, green, and blue, respectively)

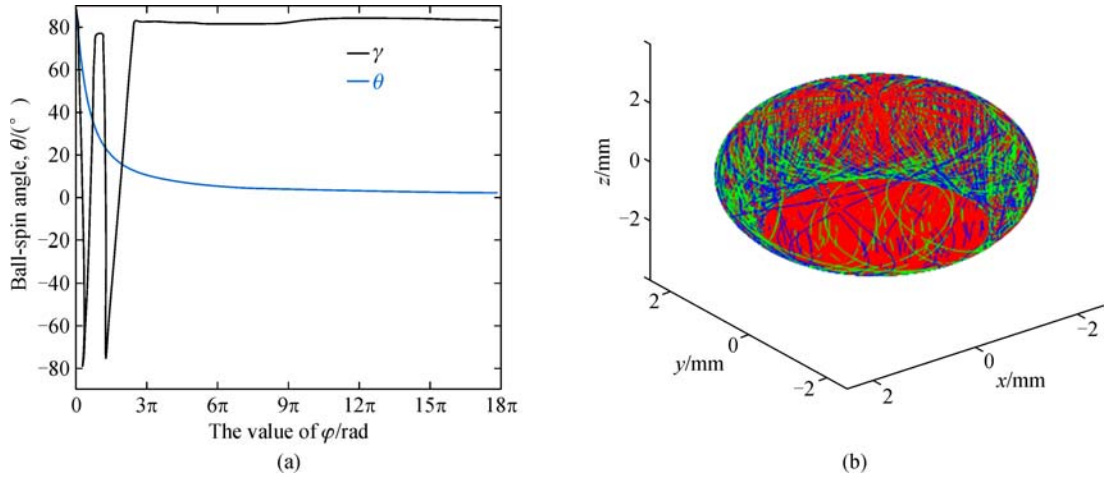

Fig. 4 Ball-spin angle and enveloped lapping trajectories in the spiral V-groove plate method. (a) Ball-spin angle; (b) enveloped lapping trajectories

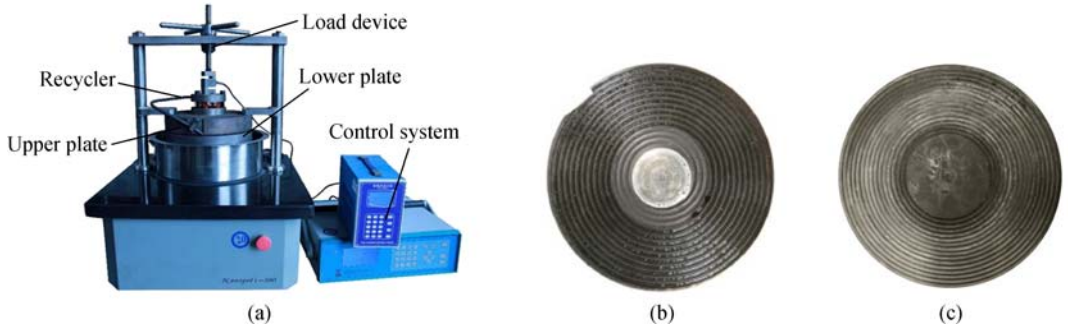

Fig. 5 Experimental rig and V-groove plates. (a) Experimental rig; (b) spiral V-groove plate; (c) concentric V-groove plate

$$R = 1.82\varphi\,(5\pi<\varphi<14\pi). \tag{18}$$

The V-groove had a 6 mm width, 6 mm depth, and 45° α and β angles. As previously mentioned, a lower φ initial value can attain greater magnitude of ball-spin angle variation. However, currently, the initial value of φ cannot be set to 0 due to the limitation of mechanical structure. Thus, in the second round, the initial value of φ was set to 5π, which is smaller than that in the first round, to achieve higher-accuracy balls.

In the first round, silicon nitride ceramic balls were used as the workpieces. The original accuracy of the used balls met the G16–G20 standards. Figures 6(a)–6(c) respectively present the initial roundness, surface roughness, and diameter of the 10 balls randomly collected from 300 raw silicon nitride ceramic balls utilized in the second round of experiments. The mean values of the roundness, surface roughness, and diameter were 0.38 μm, *Ra* 0.035 μm, and 4.7636 mm, respectively. Table 3 lists the experimental conditions. In the second round of experiments, three lapping steps, namely, coarse, middle, and fine, were performed in succession. Coarse lapping was conducted to achieve high material removal for improved roundness. Middle lapping was performed to ensure roundness and improve surface roughness. Fine lapping was conducted to eliminate surface defects and achieve high surface roughness. After each step, the 10 balls were randomly collected from the processed ones and then washed by ultrasonic cleaning, and their roundness, surface roughness, and diameter were subsequently measured.

3.2 Experimental results and discussion

Figures 7(a)–7(c) present the measured roundness values, surface roughness values, and diameters of the 10 balls, respectively, in the first round of experiments. The balls processed using the spiral V-groove plate method exhibited higher accuracy than those processed by the concentric V-groove plate method. The final mean values of the roundness and surface roughness achieved by the spiral V-groove plate method were lower by approximately 20% and 22%, respectively, than those by the concentric V-groove plate method. Furthermore, the diameter deviation achieved by the spiral V-groove plate method was $0.000073 = |6.731100 - 6.731173|$, which was lower by

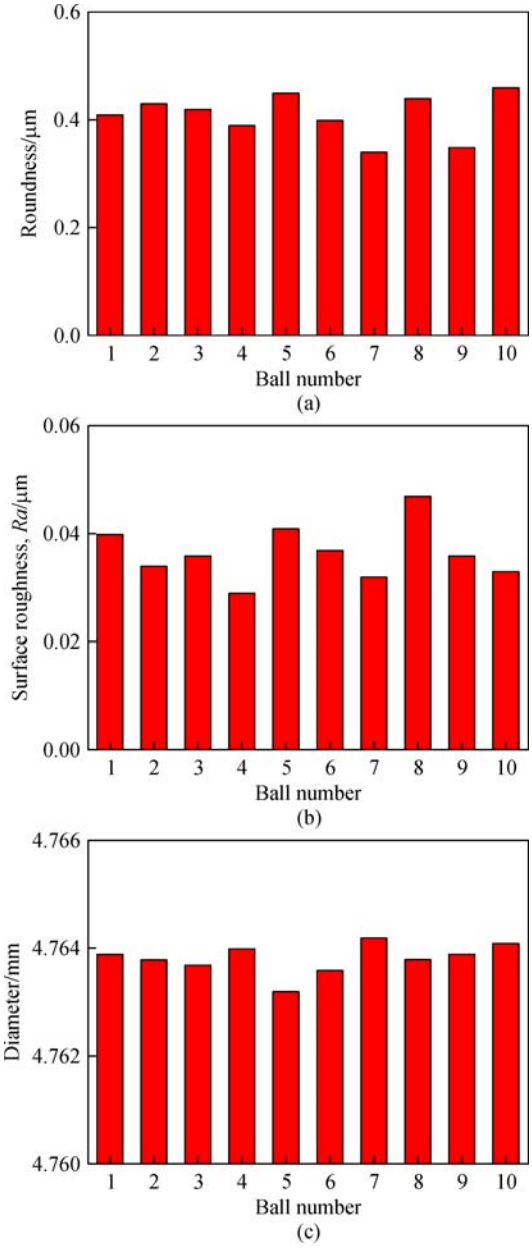

Fig. 6 Initial precision of the balls used in the experiment. (a) Initial roundness; (b) initial surface roughness; (c) initial diameter

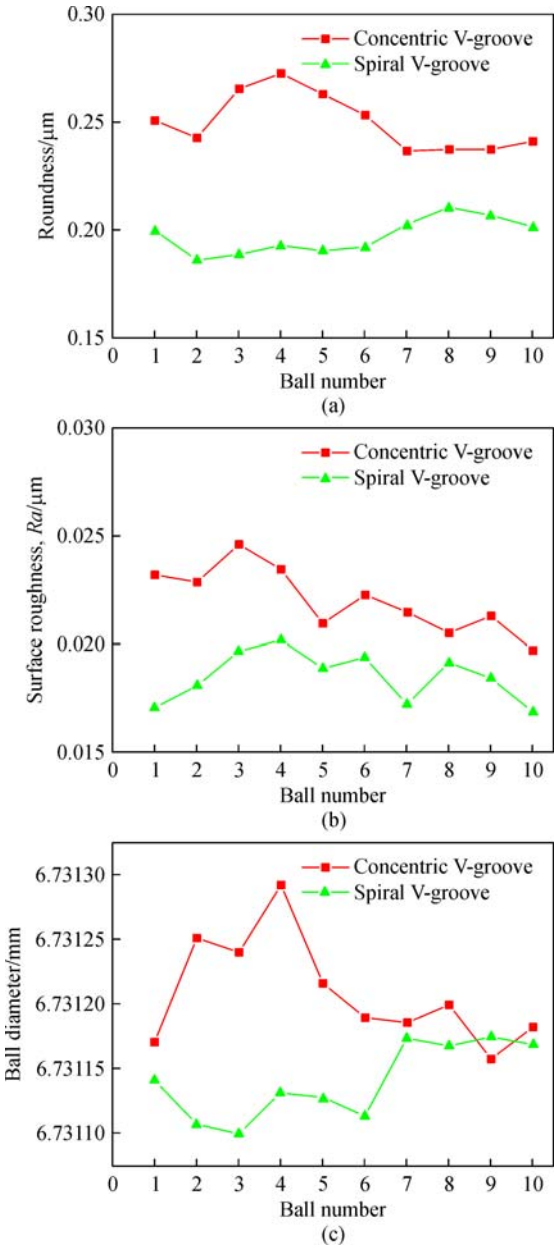

Fig. 7 Roundness, surface roughness, and diameters of the balls after the first round of processing. (a) Roundness; (b) surface roughness; (c) ball diameter

approximately 38% than that by the concentric V-groove plate method $0.00012 = |6.73116 - 6.73128|$. This result may be attributed to the fact that the ball moves for a considerably longer distance along the spiral V-groove in one cycle of the spiral V-groove plate method. Thus, material removal was relatively higher in this method compared with that in the concentric V-groove plate

Table 3 Experimental conditions

Round	Lapping step	Abrasive	Base solution	Concentration/(wt.%)	Load/N	Lower plate rotation speed/(r·min^{-1})	Time/h
First round		W3.5 diamond	Kerosene	15	150	15	6
Second round	Coarse	W2 diamond	Kerosene	15	600	30	3
	Middle	W1 diamond	Kerosene	10	300	20	3
	Fine	W0.5 diamond	Kerosene	5	150	5	6

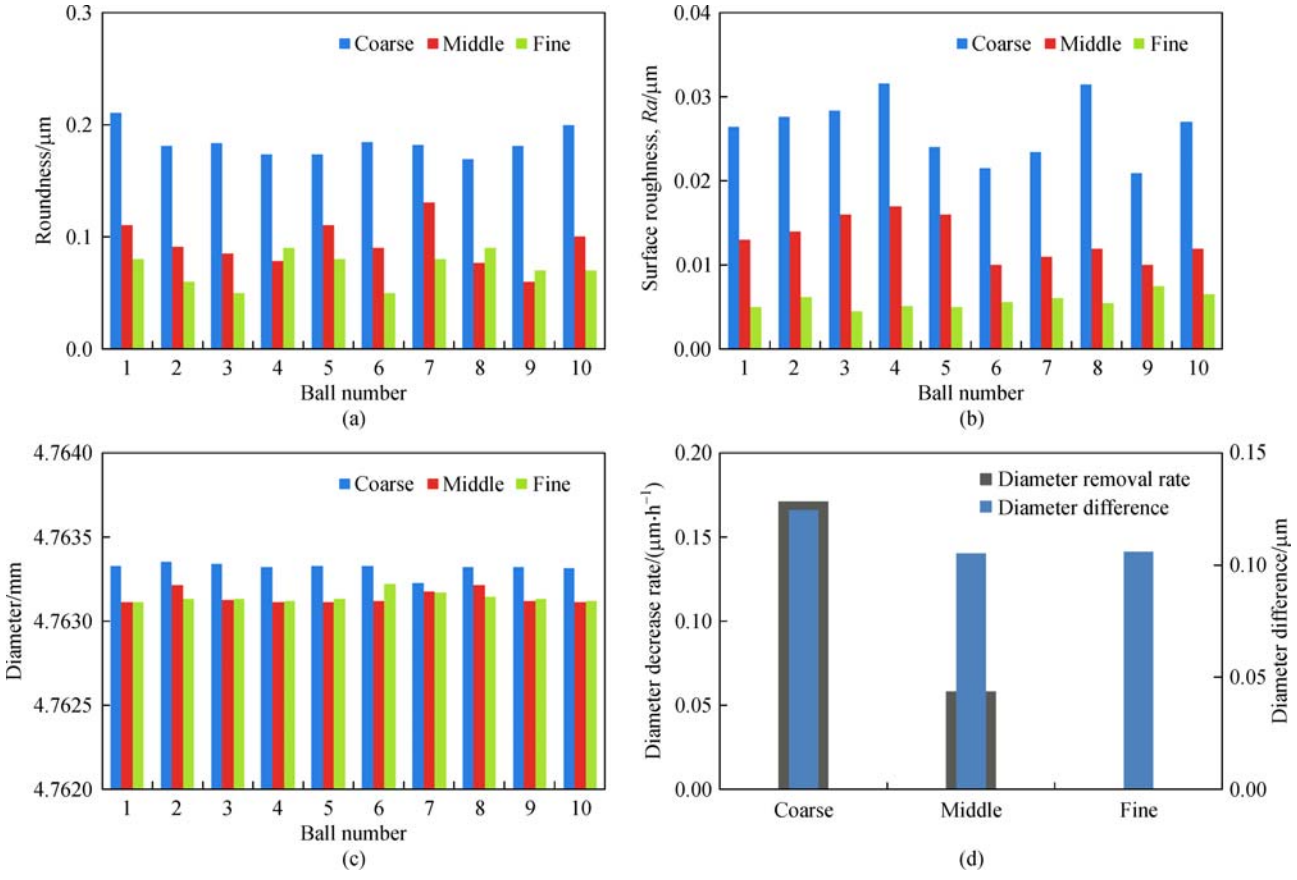

Fig. 8 (a) Roundness, (b) surface roughness, (c) diameters, (d) diameter differences and diameter decrease rates of the balls after the second round of processing

method. These results validated the performance of the new method in ceramic ball processing and demonstrated that the new method has an advantage over the conventional concentric V-groove plate method in terms of processing accuracy.

Figures 8(a)–8(d) show the roundness values, surface roughness values, diameters, and diameter decrease rates of the 10 randomly collected balls after different lapping steps in the second round of experiments. As shown in Fig. 8(a), the average value of roundness after coarse lapping was approximately 0.18 μm, reaching the G10 level. After the middle and fine lapping, the average values of roundness improved to 0.1 and 0.07 μm, respectively. The roundness of the vast majority of balls reached the G3 level. In the first two lapping steps, the process parameters were set for the primary goal of removing the material of the workpieces. Consequently, the defects on the ball surface, such as scratches and microcracks, were generated, resulting in higher roughness values. Through fine lapping, most defects were eliminated to a certain extent, and the roundness was subsequently improved.

Figure 8(b) shows that the mean roughness after coarse lapping was approximately 0.025 μm; thus, the G10 level requirement was met. The lapping load on a single ball was 2 N in this step, the abrasives completely contacted with the ball to increase the cutting depth. As a result of the high rotation speed of the lower plate, the increased cutting frequency of the abrasives increased the material removal rate. However, balls are prone to slip and collide in this situation. Thus, surface defects occurred, and surface roughness consequently increased. In middle lapping, the average value of surface roughness decreased to 0.014 μm as the abrasive size and concentration as well as the load and lower plate speed are altered. After fine lapping, the average value of the surface roughness was further improved to less than 0.0075 μm, and the minimum value was 0.0045 μm.

Figures 8(c) and 8(d) present the measured ball diameters and diameter decrease rates of the 10 randomly collected balls, respectively. The diameter decrease rate is defined as the decrease in the ball diameter per hour. In addition, Fig. 8(d) also shows the diameter difference, which is the difference between the diameters of the maximum-sized ball and minimum-sized ball. Each ball experiences nearly the same situation during coarse lapping; thus, the diameter difference reached 0.12 μm,

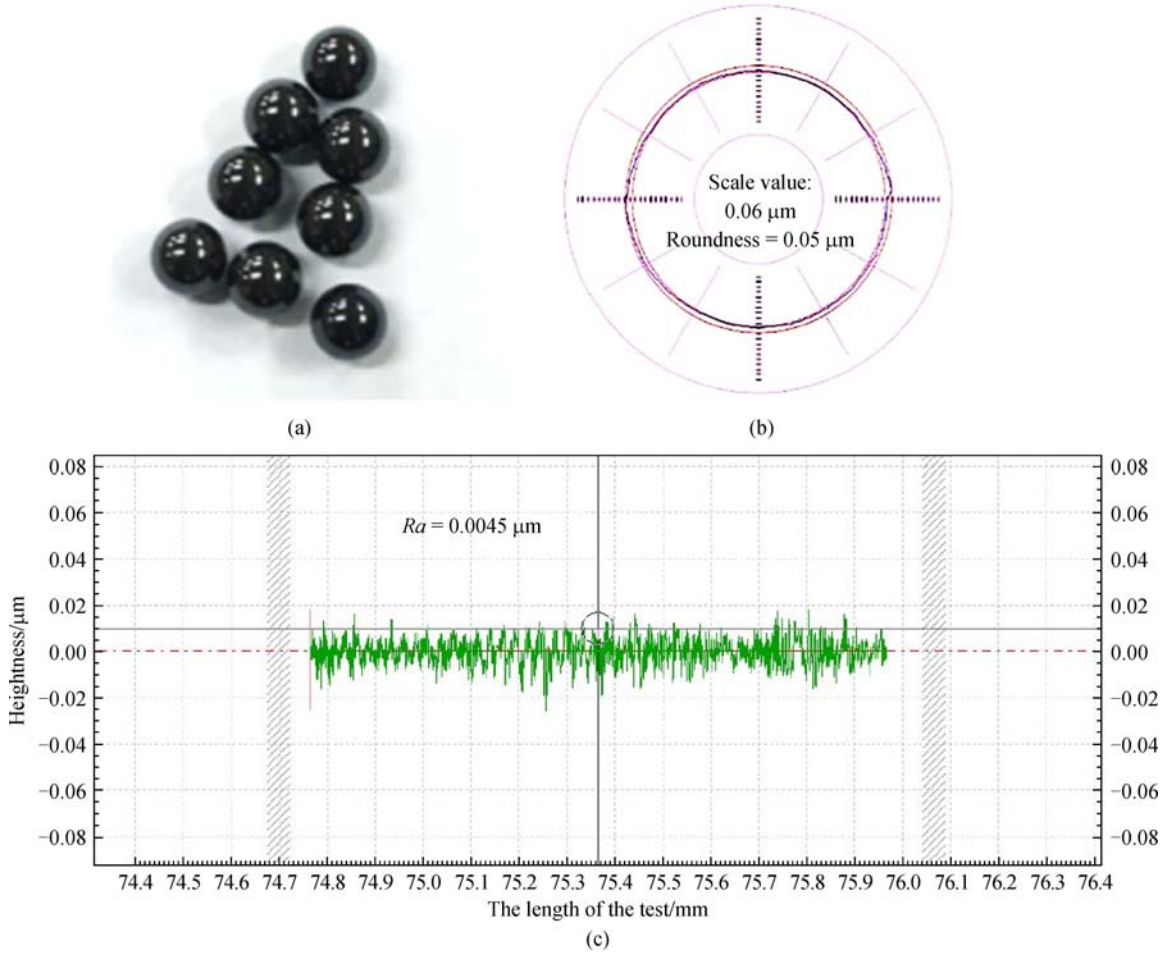

Fig. 9 Final ball appearance and measurement results of roundness and surface roughness. (a) Balls after processing; (b) typical roundness measurement result; (c) minimum surface roughness (Ra = 0.0045 μm)

reaching the G3 level; however, the diameter decrease rate was high. This outcome suggested that the proposed processing method can rapidly improve the ball diameter consistency. The diameter difference further decreased to 0.105 μm after fine lapping. However, little material was removed during fine lapping; thus, the ball diameters remained unchanged.

Eventually, the final roundness was maintained below 0.09 μm, indicating that the roundness values of a majority of the balls met the accuracy requirement of the G3 level (0.08 μm). The surface roughness and diameter difference, which reflect ball lot consistency, also reached the G3 level. Figures 9(a)–9(c) show the ball appearance after processing, the typical ball roundness measurement result (0.05 μm), and the typical ball surface roughness measurement result (0.0045 μm), respectively. These results demonstrated that the novel method can be applied to high-accuracy and high-consistency ceramic ball processing.

4 Conclusions

A spiral V-groove plate method was utilized for processing high-precision ceramic balls. After the kinematic analysis of the ball-spin angle and enveloped lapping trajectories, an experimental rig was constructed, and two rounds of experiments were conducted. The experimental results confirmed the feasibility of the novel method for processing ceramic balls. The obtained results can be summarized as follows:

1) The kinematic analysis results showed that, in the conventional concentric V-groove plate method, the ball-spin angle was constant and the lapping trajectories were three concentric rings over the ball surface. By contrast, in the novel spiral V-groove plate method, the ball-spin angles were varied and controllable, and the lapping trajectories uniformly envelope the entire ball surface.

2) The first round of experiments demonstrated that the novel spiral V-groove plate method performed better than

the conventional concentric V-groove plate method in terms of roundness, surface roughness, diameter difference, and diameter decrease rate.

3) Under the given processing parameters, ceramic balls with G3-level accuracy were achieved in the second round of experiments. The typical roundness, minimum surface roughness, and diameter difference of the balls were 0.05, 0.0045, and 0.105 μm, respectively. These results suggested that this novel method could be applied to high-accuracy and high-consistency ceramic ball processing.

Acknowledgements The authors wish to thank the National Natural Science Foundation of China for partially supporting this project (Grant No. 51375455).

References

1. Harris T A, Kotzalas M N. Essential Concepts of Bearing Technology. Boca Raton: CRC Press, 2006, 25–27
2. Bai C, Xu Q. Dynamic model of ball bearings with internal clearance and waviness. Journal of Sound and Vibration, 2006, 294 (1–2): 23–48
3. Zhuo Y, Zhou X, Yang C. Dynamic analysis of double-row self-aligning ball bearings due to applied loads, internal clearance, surface waviness and number of balls. Journal of Sound and Vibration, 2014, 333(23): 6170–6189
4. Wang L, Snidle R W, Gu L. Rolling contact silicon nitride bearing technology: A review of recent research. Wear, 2000, 246(1–2): 159–173
5. Breznak J, Breval E, Macmillan N H. Sliding friction and wear of structural ceramics. Materials Science, 1985, 20: 4657–4680
6. Zhou F, Yuan J, Lyu B, et al. Kinematics and trajectory in processing precision balls with eccentric plate and variable-radius V-groove. The International Journal of Advanced Manufacturing Technology, 2016, 84(9): 2167–2178
7. Yao W, Yuan J, Lv B, et al. Kinematics simulation of eccentric dual rotated-plates lapping for bearing balls. Advanced Materials Research, 2012, 565: 312–317
8. Cheng X, Lin F, Sun X, et al. Lapping motional trajectory analysis on sphere rotor of electrostatic gyroscope. Manufacturing Technology & Machine Tool, 2009, 30(9): 90–93 (in Chinese)
9. Yuan J, Lv B, Lin X, et al. Research on abrasives in the chemical-mechanical polishing process for silicon nitride balls. Journal of Materials Processing Technology, 2002, 129(1–3): 171–175
10. Lee R, Hwang Y, Chiou Y. Lapping of ultra-precision ball surfaces. Part I: Concentric V-groove lapping system. International Journal of Machine Tools and Manufacture, 2006, 46(10): 1146–1156
11. Kang J, Hadfield M. The effects of lapping load in finishing advanced ceramic balls on a novel eccentric lapping machine. Proceedings ofthe Institute of Mechanical Engineers. Part B. Journal of Engineering Manufacture, 2005, 219(7): 505–513
12. Yuan J, Chen L, Zhao P, et al. Study on sphere shaping mechanism of ceramic ball for lapping process. Key Engineering Materials, 2004, 259–260: 195–200
13. Umehara N, Kato K. Magnetic fluid grinding of advanced ceramic balls. Wear, 1996, 200(1–2): 148–153
14. Umehara N, Kirtane T, Gerlick R, et al. A new apparatus for finishing large size/large batch silicon nitride (Si_3N_4) balls for hybrid bearing applications by magnetic float polishing (MFP). International Journal of Machine Tools and Manufacture, 2006, 46 (2): 151–169
15. Lee R, Hwang Y, Chiou Y. Dynamic analysis and grinding tracks in the magnetic fluid grinding system: Part I. Effects of load and speed. Precision Engineering, 2009, 33(1): 81–90
16. Zhao P, Guo W, Feng M, et al. A novel lapping method for high precision balls based on variable-radius V-groove. Journal of Micro and Nano-Manufacturing, 2013, 1(4): 041007
17. Myszka D H. Machines and Mechanisms: Applied Kinematic Analysis. 4th ed. Boston: Prentice Hall, 2012, 40–65
18. Ma W. High efficiency ultra-precision grinding of ceramic balls. Dissertation for the Doctoral Degree. Saga: Saga University, 2013, 80–83